ISSN 0003-701X, Applied Solar Energy, 2023, Vol. 59, No. 6, pp. 828–835. © Allerton Press, Inc., 2023.

SOLAR ENGINEERING MATERIALS SCIENCE

Structural and Optical Properties of Thin Sb_xSe_y Films Obtained at a Substrate Temperature of 400°C

T. M. Razykov[a, b], M. S. Tivanov[c], K. M. Kuchkarov[a, b, *], R. T. Yuldoshov[a], R. Khurramov[a], S. Muzafarova[b], and D. S. Bayko[c]

[a] *Physical-Technical Institute of the Uzbekistan Academy of Sciences, Chingiz Aytmatov Str. 2B, Tashkent, 100084 Uzbekistan*

[b] *Research Institute Semiconductor Physics and Microelectronics, Yangi Olmazor 20, Tashkent, 100057 Uzbekistan*

[c] *Belarusian State University, Minsk, 220030 Belarus*

**e-mail: k.kuchkarov@mail.ru*

Received October 31, 2023; revised November 24, 2023; accepted November 29, 2023

Abstract—Sb_xSe_y thin-films were deposited by chemical-molecular beam deposition (CMBD) on soda-lime glass from antimony (Sb) and selenium (Se) precursors. Due to the separate control of Sb (between 980 and 1025°C) and Se (between 415 and 470°C) source temperature, thin films of antimony selenide with different component ratios carry out obtained. The investigation encompassed a comprehensive analysis of the elemental and phase composition, like the crystal structure, of Sb_xSe_y films. To achieve this, a combination of analytical techniques was employed, including energy-dispersive X-ray microanalysis, atomic force microscopy, Raman spectroscopy, X-ray diffraction, and scanning electron microscopy. The bandgap of the films was ascertained in the region 1.03–1.25 eV through the acquisition of absorption spectra using a spectrophotometer. This enabled the determination of the films' optical properties and facilitated further analysis of their potential applications. The physical properties of Sb_xSe_y films with various ratio were researched.

Keywords: Sb_2Se_3, optical bandgap, [*hkl*] orientation, roughness parameters, transmission reflection spectra

DOI: 10.3103/S0003701X23601552

INTRODUCTION

Binary composite semiconductors have attracted significant research interest in recent years, particularly antimony selenide (Sb_2Se_3), due to its potential as an absorbing layer for thin-film solar cells. Sb_2Se_3 is suitable for single-junction solar cells [1, 2] cause Sb_2Se_3 has strong solar absorption ($\alpha > 10^5$) [3] and has an optimal band gap of 1.1–1.3 eV. Besides, Shockley–Queisser model correspondingly, it can exhibit 31% higher theoretical conversion efficiency [4]. Currently, based of Sb_2Se_3 solar cells in a planar configuration achieve an efficiency of 10.57% [5]. Furthermore, the efficiency of Sb_2Se_3 solar cells is heavily subservient on the physical properties of the Sb_2Se_3 and the growth method employed. However, these methods often require additional processes to improve the properties of the absorbent. For example, selenization and annealing process.

One intriguing property of Sb_2Se_3 is its one-dimensional (1D) semiconductor nature. Due to its ribbon-like structure and 1D conductivity, Sb_2Se_3 films with crystal orientations (*hk*1) have demonstrated superior efficiency for photovoltaic applications compared to (*hk*0) orientations [6, 7]. As a result, by manipulating the thermodynamic parameters and approach, it is perhaps to create highly efficient Sb_2Se_3 films with the desired texture for solar cells. The anisotropic structure of the film exhibits a strong dependence on the temperature of the substrate and source, along with distinct variations in specific optical and electrical properties. Additionally, the morphology of the film surface undergoes significant alterations contingent upon the synthesis conditions [7]. Numerous studies have demonstrated the correlation between preferred orientation and device performance, often assessed through the analysis of texture coefficients (TC) derived from X-ray diffraction (XRD) patterns [8].

In our study, we propose a method to obtain Sb_xSe_y thin films with different compositions (rich in Sb or Se) without the need for additional procedures by adjusting the precursor temperatures during film growth.

EXPERIMENTAL AND RESEARCH METHODS

Sb_xSe_y thin films were deposited using separate high-purity Sb and Se granules, with purity levels of 99.999%. The temperature of the Sb source was varied from 980 to 1025°C, while the Se content during the

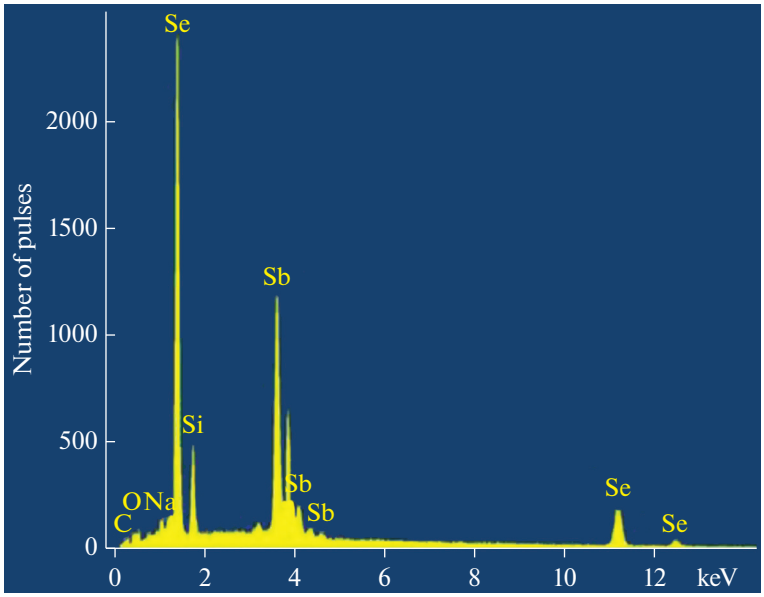

Fig. 1. Typical EDX spectrum of synthesized Sb_xSe_y thin films.

deposition process was controlled by adjusting the temperature of the selenium source in the range of 415 to 470°C. Soda-lime glass (SLG) substrates were utilized and the next step was a cleaning process using 1. acetone 2. ethanol 3. deionized water in an ultrasonic bath was performed, next by drying with N_2 gas.

The deposition of Sb_xSe_y films with a substrate temperature of 400°C was carried out at atmospheric pressure. The thickness of the thin films, ranging from 1.4 to 1.6 μm, was determined using an MIM-7 microscope. The Sb_xSe_y thin films were subjected to various characterization techniques to investigate the impact of different Sb/Se ratios on the crystal structure, morphology, and optical properties. The chemical compositions were decided using energy-dispersive X-ray (EDX) analysis Aztec Energy Advanced X-Max 80 (Oxford Instruments) spectrometer. Crystal structure analysis was performed using an Ultima IV X-ray diffractometer (Rigaku) in the grazing incidence diffraction (GIXD) geometry. In this setup, incident X-rays were directed at an angle of 1 degree, and CuKα radiation with a wavelength (λ) of 1.54178 Å was utilized. The X-ray diffraction (XRD) analysis employed the Joint Committee on Powder Diffraction Standard (JCPDS) database for reference. Raman spectra were acquired at room temperature using a Nanofinder HE (LOTIS TII) confocal spectrometer, with excitation provided by a solid-state laser (532 nm wavelength). Surface morphology and topography carry out to observe scanning electron microscope (SEM) LEO-1455 VP (Carl Zeiss) and atomic force microscope (AFM) solver Nano (NT-MDT. Reflection and transmission using a scanning spectrophotometer, specifically the PHOTON RT (Essent Optics). The optical radiation beam on the sample surface had dimensions of approximately 2 × 6 mm^2. By employing these experimental and research methods, we aimed to analyze the Sb_xSe_y thin films and investigate how different Sb/Se ratios influenced their crystal structure, morphology, and optical properties.

RESULTS AND DISCUSSION

Thin films of Sb_xSe_y with different Sb/Se ratios 0.52, 0.67, 0.70 and 0.76 were synthesized. Figure 1 shows a typical EDX spectrum of the synthesized films. In addition to the basic elements Sb and Se, a small content of Si, C, O and Na elements is observed in the spectra, which is explained by the diffusion of these elements from the SLG substrate [9, 10].

Figure 2 shows distribution of Sb and Se elements among the surface of stoichiometric ratio thin film. In Fig. 2, Sb and Se atoms were distributed uniformly. The given statement describes the results of a surface morphology investigation using scanning electron microscopy (SEM) imaging. The study focuses on Sb_xSe_y thin films deposited on a substrate known as SLG. According to the findings, all the Sb_xSe_y thin films displayed a compact surface morphology. The surface appeared smooth and dense under SEM imaging. The researchers observed that the Sb_xSe_y thin films consisted of rod-like structures. The grain sizes of these Sb_xSe_y thin films, which were in the form of rods, ranged from 0.5 to 8 microns. It means that the dimensions of the individual rod-shaped structures varied within this size range. When the Sb/Se ratios

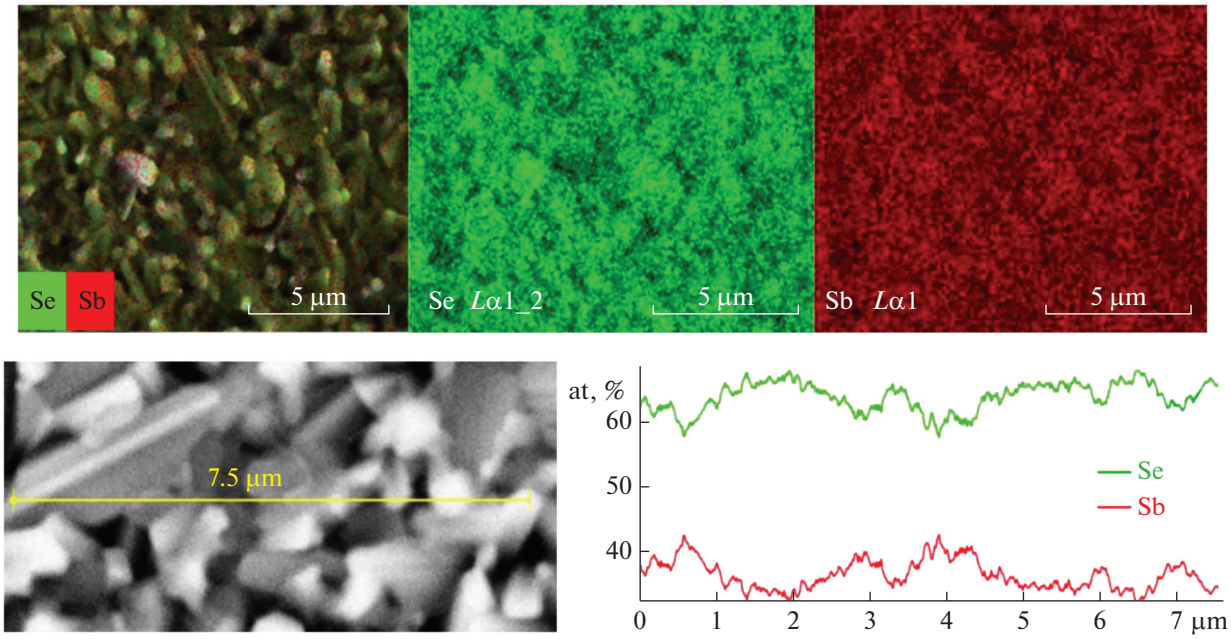

Fig. 2. Spreading of Sb and Se contents on the surface and among the exact line on the surface of 0.67 ratio Sb_xSe_y thin film.

were maintained at 0.66 and 0.7, the average diameters and lengths of the Sb_xSe_y rods were nearly the same. Specifically, the grows length of the rods are from 1 to 4 μm, and the average diameter is from 500 to 1000 nm.

At a 0.52 Sb/Se ratio, the length of the rods increased and ranged from 1 to 8 μm. Additionally, the majority of these longer rods were observed to be parallel to the substrate, indicating a specific orientation or alignment. However, at a 0.76 Sb/Se ratio, the orderly arrangement of the rods on the substrate was disturbed. It suggests that this particular composition led to a less organized or less uniform distribution of the rod-like structures on the surface. Overall, the study revealed that the Sb_xSe_y films was shown a density surface morphology, with varying sizes of grain and dimensions of rod-shaped structures depending on the Sb/Se ratio (Fig. 3).

Surface morphology studies which carried out using atomic force microscopy (Fig. 4). To appear that Sb_xSe_y films have a built surface relief in the in between ~0.15–0.27 μm average surface roughness.

The AFM (Atomic Force Microscopy) parameters for the Sb_xSe_y films are presented in Table 1. The analysis reveals that S_a and S_q of the film surface exhibit a decreasing trend as the Sb/Se ratio decreases. This implies that a under Sb/Se ratio contributes to a smoother surface. Moreover, the surface skewness, a parameter quantifying the asymmetry of the height distribution, exhibits a notable deviation from the characteristic values of a normal distribution, where zero skewness signifies a symmetrical height distribution. Instead, its value reaches 1.44, indicating an increase in asymmetry. This observation suggests a prevalence of surface peaks over valleys, potentially indicating the presence of a profile characterized by filled valleys. In contrast, the kurtosis values associated with the 0.76 Sb/Se ratio indicate a normal distribution with sharpness in the surface height distribution (S_{ka} ~ 3). However, as the Sb/Se ratio decreases, the kurtosis value increases, indicating that the surface becomes more leptokurtic [11].

GIXD measurements were conducted on different samples deposited at a substrate temperature of 400°C

Table 1. Roughness parameters of Sb_xSe_y thin films deposited at different Sb/Se ratio

Ratio Sb/Se	0.52	0.67	0.70	0.76
S_a, μm, roughness average	0.15	0.16	0.19	0.27
S_{ka}, kurtosis	7.26	4.97	4.27	3.02
S_q, μm, root mean square roughness	0.21	0.22	0.24	0.34
S_{sk}, Skewness	1.44	0.93	0.78	0.38

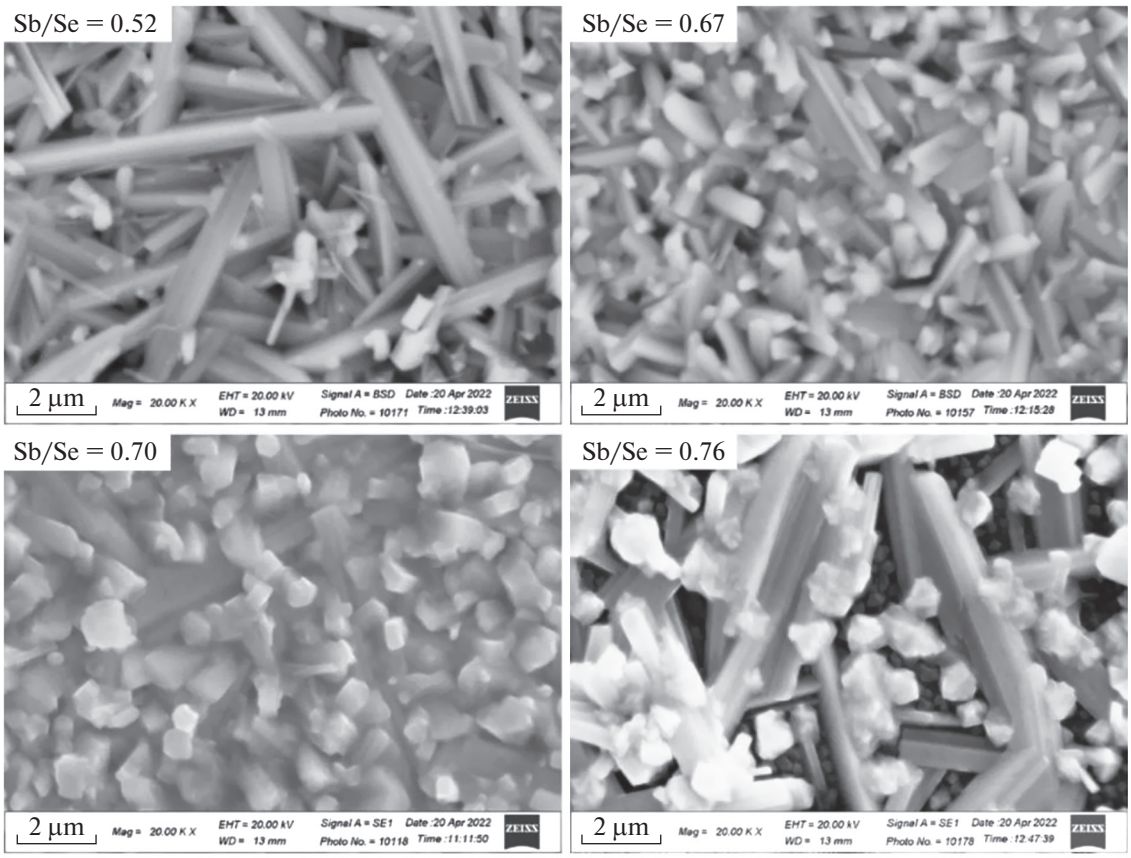

Fig. 3. SEM images of Sb_xSe_y films obtained at varied Sb/Se ratio.

to investigate the phase composition and preferred orientation of the Sb_xSe_y layers. The obtained diffraction patterns, as shown in Fig. 5a, revealed that all diffraction lines correspond to the orthorhombic Sb_2Se_3 phase (JCPDS 15-0861). The observed diffraction patterns closely matched the standard pattern which determines the good crystallinity of the films. As the Sb/Se ratio increased, peaks associated with antimony (JCPDS 85-1322) appeared on the films. Notably, for Sb/Se ≈ 0.76, a distinct peak at $2\theta = 28.67°$ corresponding to the Sb phase was clearly identifiable. The texture coefficient (TC) was calculated using the following Eq. (1). Purpose: to determine the change in orientation between thin films deposited in different Sb/Se ratios [12]:

$$TC_{(hkl)} = \frac{\frac{I(hkl)}{I_0(hkl)}}{\frac{1}{N}\sum_{i=1}^{N}\frac{I(h_ik_il_i)}{I_0(h_ik_il_i)}}, \quad (1)$$

where, the symbols $I(hkl)$ and $I_0(hkl)$ denote the diffraction peak intensities corresponding to the (hkl) planes observed in the measured X-ray diffraction (XRD) pattern of Sb_2Se_3 and the standard XRD pattern of Sb_2Se_3 (JCPDS 15-0861), respectively. The parameter N represents the total number of orientations taken into account for the calculation. A higher TC value indicates a preferred orientation of the grain along that particular direction, as depicted in Fig. 5b. Several lines were selected for texture analysis, focusing on those with the highest intensity, namely (020), (120), (130), (230), (211), (221), (240), and (061). From the analysis of Fig. 5b, it follows that the fraction of crystallites with the (hkl) orientation, most preferred for photovoltaic applications, is maximum for the ratios Sb/Se = 0.67 and 0.7.

It is known that Sb_2Se_3 films are composed of unidirectional $(Sb_4Se_6)_n$ ribbons assembled along the [001] direction due to Sb–Se covalent bonds, and $(Sb_4Se_6)_n$ ribbons are inter-ribbon are bound together by Van der Waals forces. [13, 14]. Orientation grains (hkl), consisting of $(Sb_4Se_6)_n$ ribbons, have a certain angle of inclination to the substrate, which has a better transport ability of charge carriers [15]. In addition, grains of preferential orientation consist of (hkl) planes with low surface energy. This indicate that films with grains of the preferred $[hkl]$ orientation would have a smaller breaking of covalent bonds. In other words, the grain boundaries of the preferred orientation

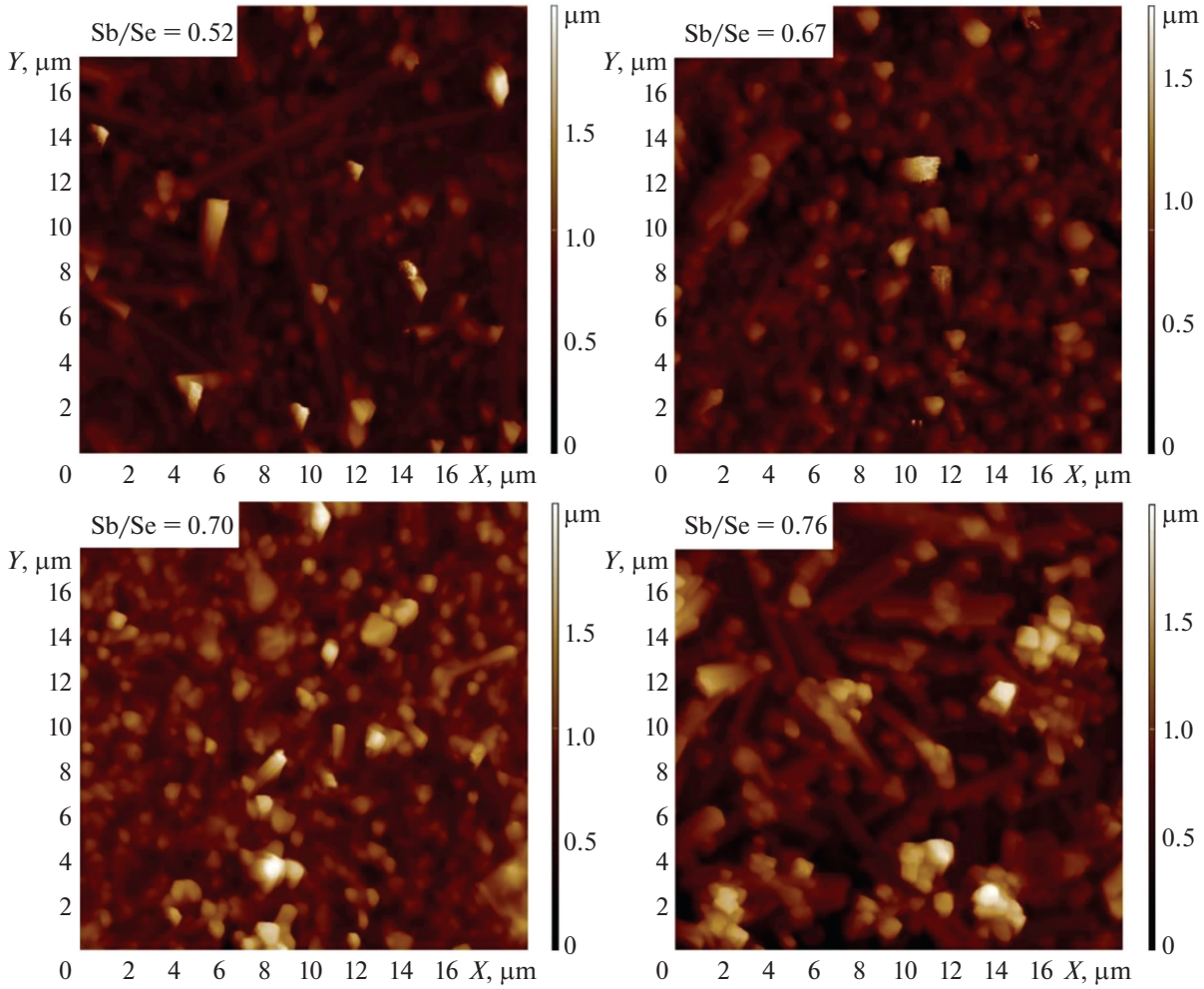

Fig. 4. AFM images of Sb_xSe_y films.

[*hkl*] can have a lower surface energy and fewer dangling bonds and are highly beneficial for reducing interface recombination and absorber transport loss [15].

Raman spectra of the Sb_xSe_y thin films exhibited characteristic vibrational modes associated with the film's structural properties. Analysis of the Raman spectra revealed significant changes in peak positions, intensities, and line shapes as a function of the Sb/Se ratio. As shown in Fig. 6, the Raman spectra exhibited peaks at presumably 79, 82, 100, 127, 153, 190, 211, and 364 cm^{-1}. The peaks in the region of 79–97 cm^{-1} can be assigned to the Sb-Se stretching mode (Ag) [16]. Additionally, these peaks may also be associated with Se in Sb_2Se_3 films with a rhombohedral structure [16]. Peaks at approximately 100, 127, 153, 190, and 211 cm^{-1} are commonly attributed to the Sb_2Se_3 phase [16–18]. The peak at around 150–153 cm^{-1} has been linked to the mode of the Sb–Sb bond [18], while the peaks at approximately 190 and 211 cm^{-1} are typically assigned to the mode of the Sb–Se–Sb bending vibrations in Sb_2Se_3 [19, 20]. Peaks in the range of 301–371 cm^{-1} may indicate the presence of Sb_2O_3 impurities [21]. Consequently, the Raman method confirmed the presence of characteristic peaks associated with the Sb_2Se_3 phase. However, it was challenging to establish the presence of the antimony phase since the characteristic peaks for antimony selenide (100 and 150 cm^{-1}) are in close proximity to the peaks observed in the spectra. Optical measurements, specifically transmission (T) and reflection (R), were performed on the Sb_xSe_y thin films deposited at various Sb/Se ratios in the spectral region of 400–3000 nm (Figs. 7a, 7b).

The optical measurements, transmission (T) and reflection (R) of Sb_xSe_y thin films deposited at various Sb/Se ratios were carried out, in 400–3000 nm spectral region (Figs. 7a, 7b). By using the optical transmission and reflection spectra, the absorption coefficient (α) of the films can be determined by employing the following equation: d—thickness of the films.

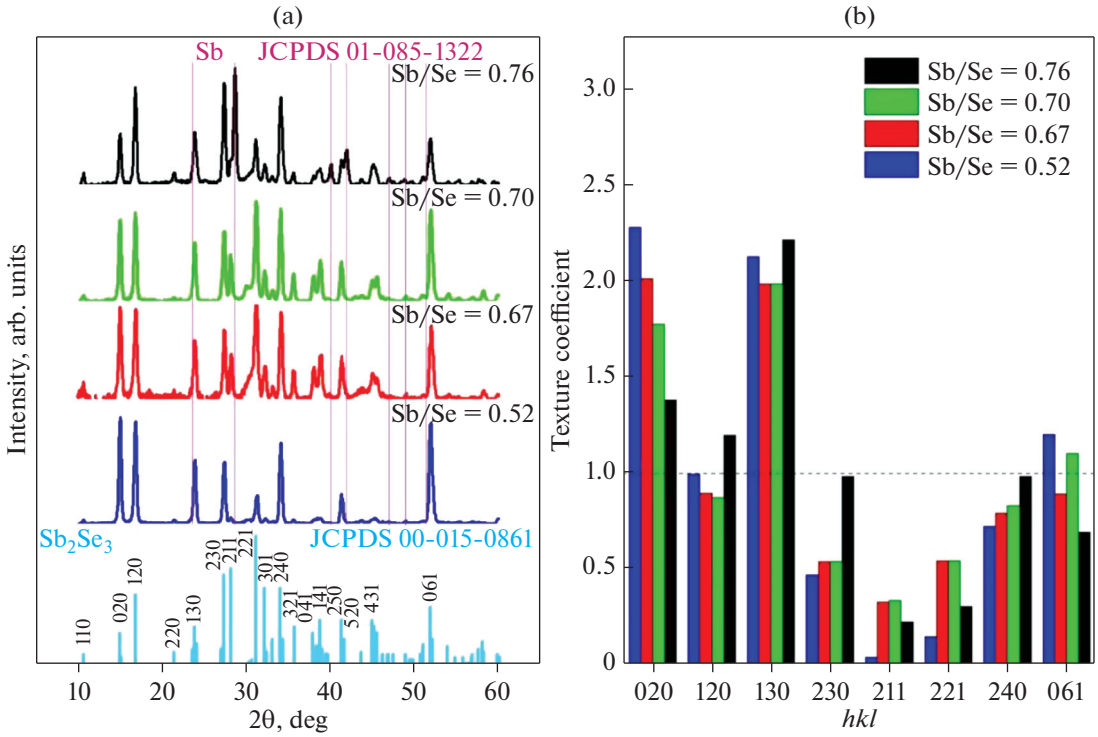

Fig. 5. (a) GIXD patterns and (b) Texture coefficients of the Sb_xSe_y thin films deposited at different Sb/Se ratios.

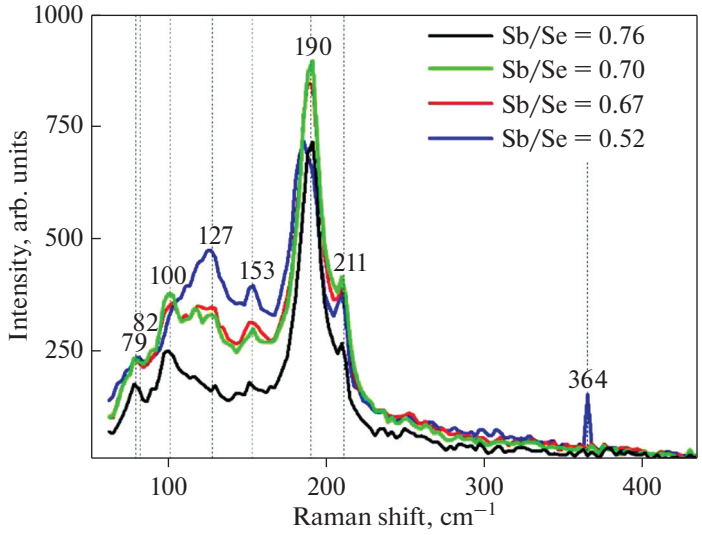

Fig. 6. Raman scattering spectra of Sb_xSe_y samples deposited at various Sb/Se ratios.

$$\alpha = -1/d\left(\frac{\sqrt{(1-R)^4 + 4T^2R^2} - (1-R)^2}{2TR^2}\right). \quad (2)$$

The optical bandgaps of films were determined by the Tauc formula [22] for direct bandgap semiconductors:

$$(\alpha h\nu)^2 = A(h\nu - E_g), \quad (3)$$

where $h\nu$—photon energy, A is a constant related to effective mass. Figure 7c shows the corresponding Tauc plots of Sb_xSe_y thin films. Band gap for varied compositional films calculated to be in the range 1.03–1.25 eV. While the maximum value of the optical bandgap corresponds to the stoichiometric ratio Sb/Se = 0.67, and minimum to the highest enrichment in antimony (Sb/Se = 0.76). Our analysis

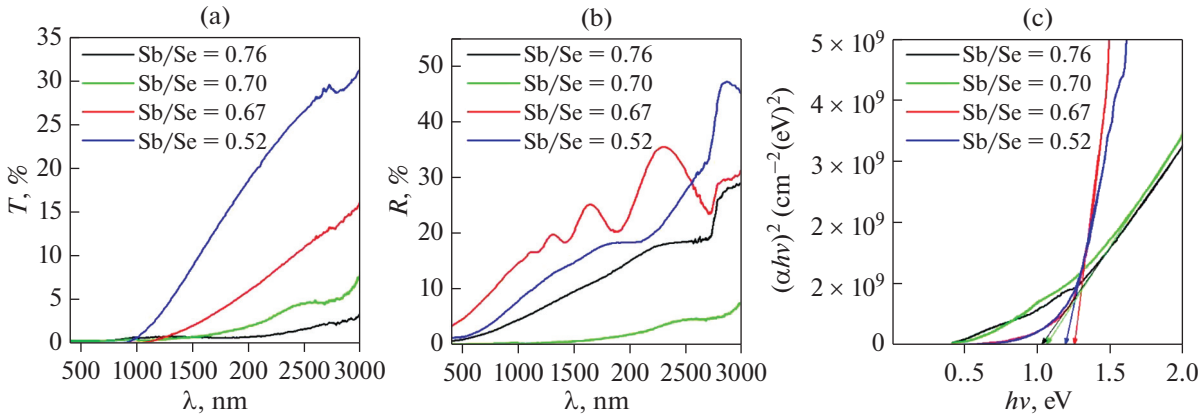

Fig. 7. (a) Transmission; (b) Reflection spectra and (c) Tauc plots of Sb_xSe_y thin films deposited at different Sb/Se ratios.

revealed a slight variation in the band gap width of the Sb_xSe_y thin films compared to the pure Sb_2Se_3 thin film, which had a band gap width of 1.15 eV [23]. This deviation can be attributed to the alteration in atomic arrangement from a disordered state to an ordered state. These data confirm previous studies that the optical and structural properties of Sb_xSe_y thin films are closely related to the Sb/Se ratio [24].

CONCLUSIONS

In conclusion, study focused on a comprehensive analysis of the optical, structural, and morphological, properties of Sb_2Se_3 films varying rations. Scanning Electron Microscopy (SEM) imaging was utilized. The SEM analysis revealed compact and uniform surface morphology across all Sb_xSe_y thin films. By studying the Energy Dispersive X-ray spectroscopy (EDX) data, grazing Incidence X-ray Diffraction analysis carry out employed to research the crystal structure of our Sb_2Se_3 films. The results demonstrated that films with microsized crystal grains exhibited a preferential orientation along the (*hkl*) direction when the composition was close to stoichiometric. Furthermore, Raman spectroscopy was conducted on the samples. Finally, the band gap of the deposited Sb_2Se_3 films was determined using Texture Coefficients based on the absorption data. In summary, our systematic investigation of Sb_2Se_3 films produced through the CMBD method, with varying compositions achieved by adjusting the Sb/Se ratio and evaporation temperature, has provided valuable insights into their morphological, structural, and optical properties.

FUNDING

This work was supported by the Basic Research Program of the Academy of Sciences of the Republic of Uzbekistan and the State Committee for Science and Technology of the Republic of Belarus (Grant No.: F21UZBG-022).

CONFLICT OF INTEREST

The authors of this work declare that they have no conflicts of interest.

REFERENCES

1. Chen, C., Bobela, D.C., Yang, Y., Lu, S., Zeng, K., Ge, C., Yang, B., Gao, L., Zhao, Y., Beard, M.C., and Tang, J., Characterization of basic physical properties of Sb_2Se_3 and its relevance for photovoltaics, *Front. Optoelectron.,* 2017, vol. 10, pp. 18–30.
2. Spalatu, N., Krautmann, R., Katerski, A., Karber, E., Josepson, R., Hiie, J., Acik, I.O., and Krunks, M., Screening and optimization of processing temperature for Sb_2Se_3 thin film growth protocol: Interrelation between grain structure, interface intermixing and solar cell performance, *Sol. Energy Mater. Sol. Cells,* 2021, vol. 225 p. 111045.
3. Zhou, Y., Leng, M., Xia, Z., Zhong, J., Song, H., Liu, X., Yang, B., Zhang, J., Chen, J., Zhou, K., Han, J., Cheng, Y., and Tang, J., Solution-processed antimony selenide heterojunction solar cells, *Adv. Energy Mater.,* 2014, vol. 4, no. 8, p. 1301846.
4. Polman, A., Knight, M., Garnett, E.C., Ehrler, B., and Sinke, W.C., Photovoltaic materials: Present efficiencies and future challenges, *Science,* 2016, vol. 352, p. 4424.
5. Zhao, Y., Wang, Sh., Li, Ch., Che, B., Chen, X., Chen, H., Tang, R., Wang, X., Chen, G., Wang, T., Gong, J., Chen, T., Xiao, X., and Li, J., Regulating deposition kinetics via a novel additive-assisted chemical bath deposition technology enables fabrication of 10.57%-efficiency Sb_2Se_3 solar cells, *Energy Environ. Sci.,* 2022, vol. 15, pp. 5118–5128.
6. Razykov, T.M., Shukurov, A.Kh., Kuchkarov, K.M., Ergashev, B.A., Khurramov, R.R., Bekmirzoyev, J.G., and Mavlonov, A.A., Morphological and structural characteristics of Sb_2Se_3 thin films fabricated by chemical molecular beam deposition, *Appl. Sol. Energy,* 2019, vol. 55, pp. 376–379.
7. Razykov, T.M., Kuchkarov, K.M., Tivanov, M.S., Ergashev, B.A., Khurramov, R., Isakov, D.Z., Olimov, A., Baiko, D.S., Polyak, N.I., Korolik, O.V., and Shari-

pov, S.D., Structural properties of Sb_xSe_y thin films obtained by CMBD for solar cells, *Appl. Sol. Energy,* 2022, vol. 58, pp. 461–465.

8. Liang, X., Guo, C., Liu, T., Liu, Y., Yang, L., Song, D., Shen, K., Schropp, R., Li, Z., and Mai, Y., Crystallographic orientation control of 1D Sb_2Se_3 nanorod arrays for photovoltaic application by in situ back-contact engineering, *Sol. RRL,* 2020, vol. 4, no. 10, p. 2000294.
9. Ko, T.Y. and Sun, K.W., Optical and electrical properties of single Sb_2Se_3 nanorod, *J. Lumin.,* 2009, vol. 129, no. 12, pp. 1747–1749.
10. Razykov, T.M., Ergashev, B.A., Yuldoshov, R.T., Mavlonov, A.A., and Kuchkarov, K.M., Production and characteristics of $(ZnSe)_{0.1}(SnSe)_{0.9}$ films for use in thin film solar cells, *Appl. Sol. Energy,* 2018, vol. 54, pp. 255–260.
11. Gadelmawla, E.S., Koura, M.M., Maksoud, T.M.A., Elewa, I.M., and Soliman, H.H., Roughness parameters, *J. Mat. Proc. Tech.,* 2002, vol. 123, pp. 133–145.
12. Zhou, Y., Wang, L., Chen, S., Qin, S., Liu, X., Chen, J., Xue, D.-J., Luo, M., Cao, Y., Cheng, Y., Sargent, E.H., and Tang, J., Thin-film Sb_2Se_3 photovoltaics with oriented one dimensional ribbons and benign grain boundaries, *Nat. Photonics,* 2011, vol. 9, pp. 409–415.
13. Filip, M.R., Patrick, C.E., and Giustino, F., GW quasiparticle band structures of stibnite, antimonselite, bismuthinite, and guanajuatite, *Phys. Rev.,* 2013, vol. 87, p. 205125.
14. Deringer, V.L., Stoffel, R.P., Wuttig, M., and Dronskowski, R., Vibrational properties and bonding nature of Sb_2Se_3 and their implications for chalcogenide materials, *Chem. Sci.,* 2015, vol. 6, pp. 5255–5262.
15. Guo, H., Chen, Z., Wang, X., Cang, Q., Jia, X., Ma, C., Yuan, N., and Ding, J., Enhancement in the efficiency of Sb_2Se_3 thin-film solar cells by increasing carrier concertation and inducing columnar growth of the grains, *Sol. RRL,* 2019, vol. 3, no. 3, p. 1800224.
16. Lei, H., Chen, J., Tan, Z., and Fang, G., Review of recent progress in antimony chalcogenide-based solar cells: Materials and devices, *Sol. RRL,* 2019, vol. 3, no. 6, p. 1900026
17. Kumar, V., Kumar, A., Romeo, A., Wiemer, C., and Mariotto, G., Raman spectroscopy and in situ XRD probing of the thermal decomposition of Sb_2Se_3 thin films, *J. Phys. Chem.,* 2021, vol. 125, no. 36, pp. 19858–19865.
18. Shongalova, A., Correia, M.R., Teixeira, J.P., Leitão, J.P., González, J.C., Ranjbar, S., Garud, S., Vermang, B., Cunha, J.M.V., Salomé, P.M.P., and Fernandes, P.A., Growth of Sb_2Se_3 thin films by selenization of RF sputtered binary precursors, *Sol. Energy Mater. Sol. Cells,* 2018, vol. 187, pp. 219–226.
19. Vidal-Fuentes, P., Guc, M., Alcobe, X., Jawhari, T., and Placidi, M., Multiwavelength excitation Raman scattering study of Sb_2Se_3 compound: Fundamental vibrational properties and secondary phases detection, *2D Materials,* 2019, vol. 6.
20. Nagata, K., Ishibashi, K., and Miyamoto, Y., Raman and infrared spectra of rhombohedral selenium, *Jpn. J. Appl. Phys.,* 1981, vol. 20, no. 3, pp. 463–469.
21. Shongalova, A., Correia, M.R., Vermang, B., Cunha, J.M.V., Salomé, P.M.P., and Fernandes, P.A., On the identification of Sb_2Se_3 using Raman scattering, *MRS Commun.,* 2018, vol. 8, pp. 865–870.
22. Yang, K., Li, B., and Zeng, G., Effects of substrate temperature and SnO_2 high resistive layer on Sb_2Se_3 thin film solar cells prepared by pulsed laser deposition, *Sol. Energy Mater. Sol. Cells,* 2020, vol. 208, p. 110381.
23. Chen, W., Li, Y., Zhou, Y., Chen, C., Luo, M., Liu, X., Zeng, K., Yang, B., Zhang, C., Han, J., and Tang, J., Optical properties of amorphous and polycrystalline Sb_2Se_3 thin films prepared by thermal evaporation, *Appl. Phys. Lett.,* 2015, vol. 107, p. 043905.
24. Liang, G.X., Luo, Y.D., Chen, Sh., Tang, R., Zheng, Z.H., Li, X.J., Liu, X.S., Liu, Y.K., Li, Y.F., Chen, X.Y., Su, Z.H., Zhang, X.H., Ma, H.L., and Fan, P., Sputtered and selenized Sb_2Se_3 thin-film solar cells with open-circuit voltage exceeding 500 mV, *Nano Energy,* 2020, vol. 73, p. 104806.